A&A manuscript no.
(will be inserted by hand later)

Your thesaurus codes are:
06 (08.14.1; 08:16:6; 09:19:1)

ASTRONOMY AND ASTROPHYSICS

Search for Discrete Refractive Scattering Events

R. Ramachandran[1], **A. A. Deshpande**[2,3], **B. W. Stappers**[4]

[1]Netherlands Foundation for Research in Astronomy, Postbus 2, 7990 AA Dwingeloo, The Netherlands
[2]Raman Research Institute, C. V. Raman Avenue, Bangalore - 560 080, India
[3]Austarlia Telescope National Facility, CSIRO, Narrabri, NSW, Australia
[4]Sterrenkundig Instituut, Universiteit van Amsterdam, NL-1098 SJ Amsterdam, The Netherlands.
email:ramach@astro.uva.nl; desh@rri.ernet.in; bws@astro.uva.nl

Abstract. We have searched for discrete refractive scattering events (including effects due to possible non-multiple diffractive scattering) at meter wavelengths in the direction of two close by pulsars B0950+08 and B1929+10, where we looked for spectral signatures associated with the multiple imaging of pulsars due to scattering in the interstellar medium. We do not find any signatures of such events in the direction of either source over a spectral periodicity range of 50 KHz to 5 MHz. Our analysis puts strong upper limits on the column density contrast associated with a range of spatial scales of the interstellar electron density irregularities along these lines of sight.

Key words: Stars: neutron; pulsars:general; ISM: structure, scattering

1. Introduction

Radio signals, during their passage through the interstellar medium, are scattered due to the irregularities in the density of free electrons (Scheuer 1968). Most often, signals from distant sources undergo strong and multiple scattering. This leads to many observable effects such as the apparent angular broadening of the source, temporal broadening of the pulse profile, diffractive and refractive scintillations. The nature of interstellar scattering at this limit and the effect on relevant observables have been studied in detail by many early workers (Lee & Jokipii 1975; 1976; Blandford & Narayan 1985; Blandford, Narayan & Romani 1984; Cordes 1986). Refractive alterations (by irregularities larger than the relevant Fresnel scale) of diffraction patterns sometimes lead to multiple images with angular separations larger than the diffraction broadening of the source (Cordes & Wolsczan 1986; Cordes et al. 1986; Goodman & Narayan 1989a,b).

If the refractive alterations become significant, then multiple imaging manifests itself in the form of periodic spectral & temporal modulation of intensity with periods smaller than the decorrelation bandwidth & decorrelation time, respectively. The probablity of multiple imaging occuring is low for a Kolmogorov spectrum of density distribution, and increases for steeper spectra as they imply dominant refractice effects (see Cordes et al. 1986 for details). However, for nearby sources, refraction angles may become comparable with the diffraction broadening even for relatively less steep density spectra. It is also likely that the diffractive scattering of the signals from some of the close-by sources is less 'multiple' in nature (with a relatively small number of speckles), mimicing in some sense the multiple imaging situation, where, with an unscattered version of the signal, only a few delayed versions interfere. Also, this may improve the detectability of a distinct signature of *single* or *discrete refractive scattering events*, where we receive, only a few discrete (diffractive) bundles of rays that correspond to different refracted (and correspondingly) delayed versions of the signal. In such a case, it appears possible to probe the properties (such as the size and density contrast) of the discrete density-irregularities responsible for the refractive/diffractive scattering, if the associated time delays can be measured.

2. Observations and Analysis

We observed two near-by pulsars, B0950+08 and B1929+10 with the aim of detecting discrete refractive scattering events. These observations were carried out with the Westerbork Synthesis Radio Telescope (WSRT) with its pulsar backend, `PuMa`. The WSRT consists of 14 dishes, each of 25-m diameter. For this observation, the delays between the dishes were compensated, and the signals were added in phase to construct an equivalent single dish of about 94 m diameter, with an antenna gain of about 1.2 K/Jy. Observations were conducted on 1999 Feb 22, and 1999 Apr 28 at a centre frequency of 382 MHz, with a bandwidth of 10 MHz. The signal voltages were Nyquist-sampled and recorded at 20 MHz in both X and Y polarisation channels. The data are quantized to represent each sample with 2 bits.

During the off-line analysis, we first performed "coherent de-dispersion" (Hankins 1971), to remove the effect of interstellar dispersion on the signals corresponding

Send offprint requests to: ramach@astro.uva.nl

to the X and the Y polarisation channels. The assumed dispersion measure values were, 2.9704 ± 0.0001 pc cm^{-3} for PSR B0950+08, and 3.1760 ± 0.003 pc cm^{-3} for PSR B1929+10. To minimise the analysis time, we gated and coherently dedispersed only the portion around the pulse (about 14% of the rotation period for PSR B0950+08, and about 8% for PSR B1929+10). The width of the gate was chosen on the basis of the known widths of the average pulse profiles. The widths at 10% of the pulse peak intensity are ∼8% & ∼6% of the periods for B0950+08 & B1929+10 respectively. The dispersion smearing within our band for both these pulsars is much smaller than the width of the gate.

In order to detect the signature of discrete refractive scattering events, we looked for significant features in the Autocorrelation (AC) function computed from the coherently de-dispersed voltage series. Since the delay we expect is of the order of microseconds (or less), there was no need to compute the AC function over a very long delay range. We computed the AC function of short stretches, each of length 102.4 μsec (2^{11} sampled points), by computing the power spectrum and inverse fourier transforming it back, after correcting for instrumental effects. There is also another important reason for restricting the length of the AC functions to such a short length. PSR B0950+08 is known to show significant short-time scale features (microstructure) in its pulse window. The typical time scale for these features is about 175 μsec (Hankins 1972). Since it is important to minimise the contribution of this microstructure to our AC function, we chose our transform lengths to a value of 102.4 μsec, which is smaller than the microstructure time scale.

Since the input voltage time series is a "real-function", the power spectrum computed over 20 MHz would be (real &) symmetric about the 'zero' frequency. Any discrete feature in the AC function manifests itself as a "fringe pattern" (or a periodic modulation) in this power spectrum. Since the phase of such a pattern is also of some interest, while taking the inverse fourier transform we use only a one-sided power spectrum (say, frequencies ≥0), such that the AC function thus obtained contains both, amplitude & phase, information (i.e. this AC function would be a complex function) associated with any spectral modulation.

It should be emphasised here that we compute the autocorrelation of the voltage series, and not the "detected" (i.e., intensity) series. It is easy to see that the fourier transform of the latter would correspond to a *fluctuation spectrum* of the intensity, rather than the *radio frequency spectrum* we wish to study. This allows us not only to reduce considerably the effect of any intrinsic fluctuations like microstructure, but also to measure more directly the time delays of interest.

Within the pulse window, autocorrelation functions were computed by taking half-overlapping time sections of 2^{11} points. In order to improve the signal-to-noise ratio, all these autocorrelation functions were added together with weights given by the square of their individual signal-to-noise ratios (which is estimated from the mean power in the power spectrum). Furthermore, we repeat this procedure over many pulses and average all the individual autocorrelation functions, to compute the final autocorrelation function.

2.1. Instrumental and other spurious effects

While computing the mean of the power spectrum, we made sure to identify all the spurious interference signals, and to not include them in the calculation. We replaced the spectral channel contributions affected by the narrow-band interference by the value corresponding to the mean contribution from the unaffected channels, so that they do not corrupt the autocorrelation function estimation. It was very important to remove such contributions. Otherwise they bias the mean estimations, and can also introduce strong intermodulation products.

2.1.1. Instrumental response function

The estimations of two major instrumental effects which had to be compensated for are an essential part of our analysis. The two effects are related to, (1) the intrinsic band shape of the instrument, and (2) the *front-end response*. The reason for considering the front-end (signal path from the telescope up to the first amplifier) as a separate entity is that a very significant fraction of the system noise, contributed by the first amplifier, does not sample the spectral response of the front-end. This means that the spectral response estimated on the basis of the off-pulse region of the data set can not be used to adequately correct for the instrumental response to the sky/pulsar signal.

We model the instrumental response function as follows:

$$B_{\rm on}(\nu) \;=\; \langle B_{\rm off}\rangle(\nu)\;\left[1 \;+\; \left(\frac{A_{\rm on} - \langle A_{\rm off}\rangle}{\langle A_{\rm off}\rangle}\right)\; D(\nu)\right] \qquad (1)$$

Here, $B_{\rm on}(\nu)$ is the on-pulse bandshape as a function of frequency (obtained for a given stretch of 2^{11} points), $\langle B_{\rm off}\rangle(\nu)$ is the average off-pulse bandshape as a function of frequency, $A_{\rm on}$ is the mean of the instantaneous on-pulse bandshape, and $\langle A_{\rm off}\rangle$ is the mean of the average off-pulse bandshape. $D(\nu)$ is the front-end response function.

In order to correct for the above, we pre-computed a high-signal-to-noise ratio average off-pulse band shape function, $\langle B_{\rm off}\rangle(\nu)$. We also pre-computed the function $D(\nu)$ by inverting the above equation and by estimating its suitably weighted average as

$$D(\nu) \;=\; \frac{\sum_{i=1}^{M}\left[\frac{B_{\rm on}(\nu)}{\langle B_{\rm off}\rangle} - 1\right]\; w_i}{\sum_{i=1}^{M} {w_i}^2} \qquad (2)$$

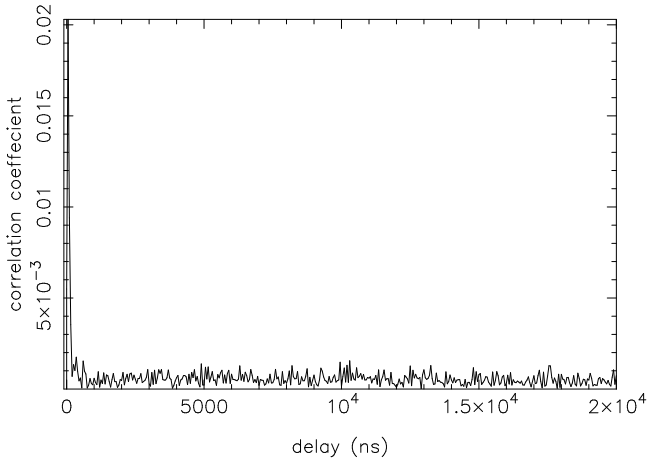

Fig. 1. Autocorrelation function computed for PSR B0950+08. This function is based on the analysis of 632 pulses observed at a centre frequency of 382 MHz, with 10 MHz bandwidth. See text for details.

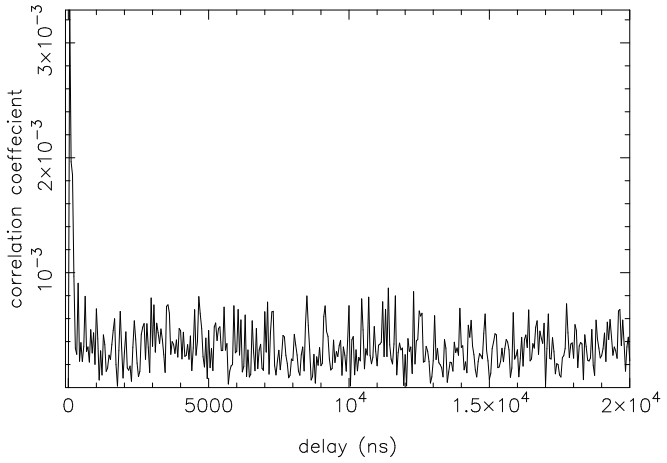

Fig. 2. Autocorrelation function computed for PSR B1929+10. This function is based on the analysis of 700 pulses observed at a centre frequency of 382 MHz, with 10 MHz bandwidth. See text for details.

here, $M = (N_{\rm str} \times N_{\rm pul})$, with $N_{\rm str}$ and $N_{\rm pul}$ being the number of stretches in a pulse & the number of pulses considered for the analysis, respectively and $w_i = [A_{\rm on}/\langle A_{\rm off}\rangle - 1]$ is a quantity proportional to the signal-to-noise ratio of the pulse in the corresponding stretch.

Then, before computing the autocorrelation functions, we compensated for the instrumental effects to obtain

$$B_{\rm on}(\nu) \;=\; [B'_{\rm on}(\nu) \;-\; \langle B_{\rm off}\rangle(\nu)] \,/\, [D(\nu)\;\langle B_{\rm off}\rangle(\nu)] \qquad (3)$$

where, $B'_{\rm on}(\nu)$ is the uncorrected power spectrum. The corrected power spectrum, $B_{\rm on}(\nu)$, is inverse fourier transformed to estimate the autocorrelation as function of delay τ. The front-end response function, $D(\nu)$, was determined using the pulsar observation itself, and a smooth functional form (with a low-order polynomial) fitted to the estimate was used for the correction described. This ensured that any fine-scale spectral modulation in the pulsar signal was not removed as part of the instrumental response.

3. Results

We analysed 632 pulses for PSR B0950+08, and 700 pulses for PSR B1929+10. The final AC functions are normalised according to the following procedure.

As described in section 2, in each stretch, we have $N = 2^{11}$ samples (102.4 μsec). With the root-mean-square value (r.m.s.) of the initial voltage time series $\sigma_\circ$, the r.m.s. of the noise in the real and the imaginary parts of the normalised AC function is $\sigma \;=\; \sqrt{2/N}$.

In our procedure, many such AC functions are added together. The number of AC functions in either the X or the Y polarisation channel is given M as defined above. The final AC function $\langle C(\tau)\rangle$ is computed by a weighted average given by,

$$\langle C(\tau)\rangle \;=\; \frac{\sum_{i=1}^{M} W_i\; C_i(\tau)}{\sum_{i=1}^{M} W_i} \qquad (4)$$

where $C_i(\tau)$ is the AC function for the $i^{\rm th}$ stretch and the weightage W_i $(={w_i}^2)$ is proportational to the square of the signal-to-noise ratio of the pulsar contribution in that 102.4μsec stretch.

The r.m.s. of the real and imaginary parts of the normalised final AC function is $\sigma_f \;=\; \sigma/\sqrt{M_{\rm eq}} \;=\; \sqrt{2/(N \times M_{\rm eq})}$, where $M_{\rm eq}$ is the equivalent number of ACFs averaged ($\leq M$). If the weights for all the stretches are equal, then $M_{\rm eq} = M$.

Figures 1 & 2 give the normalised amplitude of the final (average complex) AC function for PSRs B0950+08 and B1929+10, respectively. Note that the AC function resulting from this analysis has a null at 'zero-delay', i.e. the feature corresponding to the mean spectral contribution is removed. As our radio frequency bandwidth is 10 MHz, in principle, we should be able to measure any feature whose time delay is greater than ∼100 ns. However, due to a finite residual in the instrumental response which remains uncompensated despite our detailed modelling, the minimum delay for our ACF estimation is ∼200 ns. As we can see, there is no significant feature in the AC functions beyond this delay. This indicates an absense of a) prominant discrete refractive scattering events as well as b) non-multiple diffractive scattering along both lines of sight.

4. Discussion

In our observations, we have looked for fine periodic spectral structure across a bandwidth not very much wider than the decorrelation bandwidth. Also, the data span used corresponds to an interval smaller than the decorrelation time for diffractive scintillations of both pulsars. Thus our analysis uses data over at most a couple of diffractive scintles, and is therefore less affected by any possible decoherence due to variation of the diffractive phase from scin-

tle to scintle. Considering the possibility that the spectral modulation (which we have searched for) could drift across the spectrum with time (although the drift is expected to be small over our data span), we have also examined the average of ACF amplitudes alone (instead of its vector equivalent) so as to avoid possible 'dephasing' of any otherwise detectable ACF feature. Again, no significant feature was apparent.

We interprete our *null* result as indicating an absense of strong refraction gradients across the scattering screens. Our results also suggest that the diffractive scattering is rather 'multiple', i.e. the diffraction image consists of a large number of 'speckles' or sub-images. While the former indication can be understood simply as the result of a non-steep spectrum of density irregularities with an 'inner scale' much smaller than the Fresnel scale, we attempt to quantify our conclusion using the following simple-minded picture.

Crossing of refracted ray bundles is a necessary condition for multiple imaging (see Cordes et al 1986 for more details). This condition is not met if the differential refraction across a given transverse scale is less than its angular size as seen from the observer's location. Let us consider a refracting screen mid-way along a pulsar sight-line, and assume that two wavefronts, one of which is refracted significantly more (by, say, an angle θ) than the other, describe the refractive effect of the scattering screen over a transverse separation 'a'. For a difference ΔDM in the electron column density sampled by the two paths, the two wavefronts will cross if $\Delta DM \geq (8\pi/Lr_e)(a/\lambda)^2$, where r_e is the classical electron radius, L is the distance to the pulsar, and λ is the wavelength of observation. For the situation described here, it is easy to show that the geometric delay difference will be equal to the differencial dispersion delay corresponding to ΔDM.

Figure 3 shows the above mentioned limits on column density contrast ΔDM (in units of pc cm^{-3}) associated with large-scale irregularity as a function of transverse scale 'a' (in AU) for the two pulsars, B0950+08 (solid line) and B1929+10 ('dash' line). The distances to these two pulsars are assumed to be 120 pc and 170 pc, respectively. The vertical axis (right side) indicates the associated relative delay (including the dispersion contribution) for comparison with our measurements. The horizontal axis (top side) is also marked with relative epochs (for the line of sight to traverse a mid-way transverse distance of a) corresponding to a proper motion of 100 km/s. It would be instructive to compare these limits on the structure function of dispersion measure when suitable direct measurements of changes in DM in the two directions may become available in future. It is also worth mentioning that the characteristic delay associated with diffractive scattering of the two cases (B0950+08 & B1929+10) are 4.7 & 0.08 μsec, respectively, and would translate to scattering disk size of 0.8 & 0.12 AU, respectively. The Fresnel scale, for comparison, is $\sim 10^{-2}$ AU.

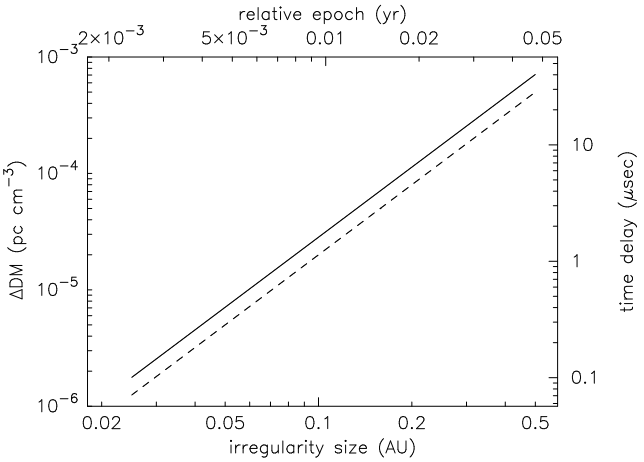

Fig. 3. Upper bounds to the structure function of dispersion measure. The solid line is for PSR B0950+08, and the 'dash' line is for B1929+10. See text for details.

It is worth mentioning that the power spectrum of irregularities in the direction of B1929+10 appears relatively steep (Bhat, Gupta & Rao 1999) and hence the refractive effects can be expected to be dominant, relatively speaking. Also, the multipath scale (defined by the apparent size of the scatter-broadened image) when viewed in units of the Fresnel scale is an order of magnitude smaller for B1929+10 than that for B0950+08, indicating correspondingly weaker and less multiple scattering. However, it is not clear as to how much of this apparent difference is due to the possible differences in the fractional distance to the scatterer (i.e. the scatterer location may be at one end in the case of B1929+10 instead of mid-way as we have assumed). It should be emphasised here that the refractive effects are highly episodic. So our (*null*) results on these two pulsars, and the implied constraints (as in Figure 3), while being indicative, should be viewed as applying strictly only to the epochs of our observations.

To summarise, radio signals emitted by very near-by sources may be scattered by discrete refractive irregularities that alter the diffraction patterns significantly, or may undergo 'non-multiple' diffractive scattering. Finding distinct spectral signatures of such events allows us to study the size and the density contrast of such large-scale irregularities. We have looked for such signatures in the signals from PSR B0950+08 and PSR B1929+10, but found no corresponding ACF feature significantly above the noise threshold (7σ) of 2×10^{-3} and 1.3×10^{-3}, respectively. The absence of any such signature/event in the observed data suggests useful limits on the structure function of dispersion measure corresponding to a wide range of refractive scales in the two lines of sight (as sampled at the epoch of our observations).

Acknowledgements

The software code for coherent de-dispersion was developed by Dipankar Bhattacharya, along with one of the authors (RR). We thank our referee, Jim Cordes, for valuable critical comments that have helped us in improving the paper significantly.

References

Bhat N.D.R., Gupta Y., Rao A. P. 1999, ApJ, 514, 249
Blandford R. D., Narayan R., 1985, MNRAS, 213, 591
Blandford R. D., Narayan R., Romani R. W., 1984, A&A, 5, 369
Cordes J. M., 1986, ApJ, 311, 183
Cordes J. M., Pidwerbetsky A., Lovelace R. V. E. 1986, ApJ, 310, 737
Cordes J. M. & Wolszczan A. 1986, ApJ, 307, 27
Goodman J. & Narayan R. 1989a, MNRAS, 231, 97
Goodman J. & Narayan R. 1989b, MNRAS, 238, 995
Hankins T. H., 1971, ApJ, 169, 487
Hankins T. H., 1972, ApJ, 177, 11
Lee L. C., Jokipii J. R., 1975, ApJ, 201, 532
Lee L. C., Jokipii J. R., 1976, ApJ, 206, 735
Scheuer P. A. G., 1968, Nature, 218, 920